RSC Advances

PAPER

View Article Online
View Journal | View Issue

Cite this: *RSC Adv.*, 2021, **11**, 19560

How do the doping concentrations of N and B in graphene modify the water adsorption?

Thi Tan Pham,†[ab] Thanh Ngoc Pham,†[ab] Viorel Chihaia,[c] Quang Anh Vu,[ab] Thuat T. Trinh,[d] Trung Thanh Pham,[e] Le Van Thang*[ab] and Do Ngoc Son*[ab]

Received 24th February 2021
Accepted 14th May 2021

DOI: 10.1039/d1ra01506k

rsc.li/rsc-advances

Understanding the interaction of water and graphene is crucial for various applications such as water purification, desalination, and electrocatalysis. Experimental and theoretical studies have already investigated water adsorption on N- and B-doped graphene. However, there are no reports available that elucidate the influences of the N and B doping content in graphene on the microscopic geometrical structure and the electronic properties of the adsorbed water. Thus, this work is devoted to solving this problem using self-consistent van der Waals density functional theory calculations. The N and B doping contents of 0.0, 3.1, 6.3, and 9.4% were considered. The results showed that the binding energy of water increases almost linearly as a function of doping content at all concentrations for N-doped graphene but below 6.3% for B-doped graphene. In the linear range, the binding energy increases by approximately 30 meV for each increment of the doping ratio. Analyses of the geometric and electronic structures explained the enhancement of the water–graphene interaction with the variation in doping percentage.

1. Introduction

The interface between water and graphene plays an important role in diverse applications such as wetting, water purification, desalination, and electrocatalysis owing to its frictionless properties.[1,2] The water–graphene interface has been intensively investigated by experimental and computational methods.[2–10] Experimentally, the interface can be studied by measuring static water contact angles, providing macroscopic understanding, and different values of the water contact angles were reported for water droplets on graphene.[1–4] The discrepancy in the reported data originates from several factors, *i.e.*, the number of graphene layers, the underlying substrate, and the effects of doping. Hong *et al.* showed that the supporting substrate and physical doping by applying a voltage can unambiguously affect the hydrophilicity of graphene, which was later confirmed by Ashraf *et al.*[3,4] Both studies claimed that the origin of the physical doping-induced wettability of graphene is the shift of the Dirac point away from the Fermi level of graphene. To provide an atomistic understanding, density functional theory (DFT) calculations have been widely employed to investigate the adsorption of water on graphene.[5–10] Nevertheless, the different computational parameters result in a discrepancy in the binding energy (E_b) of the water monomer on graphene, which is mainly due to lack of treatment of the van der Waals interactions. By using the conventional GGA-PBE method, the E_b is 30 meV, whereas the vdW-DF2^{C09x} result[6] is 80 meV, which is more consistent with the random-phase approximation (98 meV) and the diffusion Monte Carlo method (100 meV).[8] The variance between the GGA-PBE and vdW inclusive methods is about 50 meV; however, Brandenburg *et al.* found that a change in E_b of H_2O on graphene of 50 meV leads to the graphene surface changing from hydrophobic to hydrophilic.[8] This highlights the importance of using van der Waals inclusive DFT methods to study the water–graphene interaction.[7,8] To elucidate the wetting dynamics of water on graphene, classical molecular dynamics simulations were employed.[11,12] Andrews *et al.* pointed out that at rather low coverage, water molecules tend to spread out and form water layers on graphene, whereas water nanodroplets are formed when more water molecules are exposed.[11] Similarly, Akaishi *et al.* also found that water forms a double layer covering the entire graphene surface, followed by the formation of three-dimensional water clusters. Their results indicated that the pristine graphene itself exhibits hydrophilicity and the stabilization of the water double layer on graphene leads to the hydrophobicity observed in experiments.[12] The predictions of two previous theoretical studies have been proved by recent experiments on the water–graphite interface.[13]

[a]*Ho Chi Minh City University of Technology, 268 Ly Thuong Kiet Street, Ward 14, District 10, Ho Chi Minh City, Vietnam. E-mail: dnson@hcmut.edu.vn; vanthang@hcmut.edu.vn*

[b]*Vietnam National University Ho Chi Minh City, Quarter 6, Linh Trung Ward, Thu Duc District, Ho Chi Minh City, Vietnam*

[c]*Institute of Physical Chemistry "Ilie Murgulescu" of the Romanian Academy, Splaiul Independentei 202, Sector 6, 060021 Bucharest, Romania*

[d]*Department of Civil and Environmental Engineering, Norwegian University of Science and Technology, NO-7491 Trondheim, Norway*

[e]*Namur Institute of Structured Matter (NISM), Department of Physics, University of Namur, 61 Rue de Bruxelles, B-5000 Namur, Belgium*

† These authors contributed equally to this work.

Wang *et al.* experimentally observed a monolayer of water grown on the graphite surface using STM imaging.[13] By using DFT calculations, they also found that all water molecules within this monolayer form a strong hydrogen bonding network, giving rise to the stabilization of this water monolayer.

Compared to the wealth of information concerning water on pristine graphene, the physical properties of water on nitrogen (N) and boron (B)-doped graphene are not fully understood yet.[14,15] N-doped graphene quantum dots showed hydrophilicity (hydrophobicity) with mono-layered (multi-layered) structures.[16] Graphene doped with boron has been synthesized and used in various applications.[17] Dai *et al.* theoretically investigated the adsorption of water and gases on single site X-doped graphene (X = B, N, Al, and S) using the GGA-PBE method, and N and B doping enhanced the adsorption strength of water.[18] Yang *et al.* studied water/fluorinated graphene using DFT calculations with the vdW-DF functional and found that fluorine doping could increase the E_b of the adsorbed water and change the water dipole moment.[19] Recently, Xu *et al.* investigated water on hydrogenated pyridinic N-doped, graphitic, and pyrrolic N-doped graphene using the GGA-PBE approximation with Grimme's D2 dispersion correction.[20] It was found that both the E_b and the orientation of the water molecules are significantly altered upon N doping. Cardozo-Mata *et al.* also studied water dimers on the N terminated vacancies of graphene and found that the interaction mainly originates from hydrogen bonding between water H and N.[21] All of the previous reports considered water adsorption on N- and B-doped graphene at a specific doping content and on the N terminated graphene edges and defects; however, the influences of the N and B doping content on the water–substrate interaction remain unknown. Therefore, this work addresses this issue by systematically considering the water adsorption on graphene with N and B doping at the graphitic sites and low concentrations of 0.0, 3.1, 6.3, and 9.4%. Using DFT calculations with the rev-vdW-DF2 functional, we elucidated a microscopic picture of the structural–electronic property relationships for water–graphene systems. There are several types of doping in graphene. The graphitic type refers to replacing the C atoms in graphene with dopant atoms like N and B, which retains the honeycomb structure of perfect graphene, and the pyridinic and pyrrolic types indicate doping accompanied by the creation of vacancies and edges. The graphitic type of doping[22–25] was considered in the current work because it exhibits higher stability than the pyridinic and pyrrolic types[26,27] and also has potential applications in fuel cells, Li-ion batteries, photocatalysis, and electrochemical sensing.[28] Clarification of the hydrophilicity and hydrophobicity of water on N,B-doped graphene with variation of the doping content is out of scope. Also, we only focused on doping with single components of N and B without mixing of these elements.

2. Computational details

All our DFT calculations were performed within the periodic supercell approach using the Quantum ESPRESSO package.[29] Core electrons are represented by Vanderbilt's ultrasoft pseudopotentials[30] with the GBRV library,[31] whereas the valence states were expanded in plane waves with cut-off energies of 50 and 600 Ry for wave functions and augmented charge densities, respectively. We used the rev-vdW-DF2 exchange–correlation functional,[32] which has been shown to give reasonable accuracy for water on carbon materials,[33] as well as other systems.[34–37] All atoms are allowed to relax until the force acting on them is less than 0.02 eV Å^{-1}. A Γ-centered 6 × 6 × 1 *k*-point mesh is used for structural optimizations. To accurately calculate the density of states (DOS), a Γ-centered 16 × 16 × 1 *k*-point mesh is employed. To estimate the vacuum level and thus the work function accurately, we employed dipole moment correction to eliminate the spurious electric field in the surface normal direction.[38] This correction is used only for the calculation of the work function, and it is omitted during structural optimization.

The pristine and doped graphene films were modeled by using a unit cell of lateral (4 × 4) periodicity composed of 32 C atoms with a vacuum of 18 Å in the normal surface direction. To evaluate the stability of graphene doped with N and B, the formation energy is calculated by

$$E_f = E_{gra} - N_X \times \mu_X, \quad (1)$$

where E_{gra}, μ_X, and N_X stand for the total energy of the graphene system, the chemical potential of element X, and the number of atoms of element X (X = C, N, B), respectively. We used the total energy per atom of graphene, gas-phase N_2, and bulk α-rhombohedral boron, represented by μ_C, μ_N, and μ_B, respectively.

The binding energy of water on pristine and doped graphene is estimated by

$$E_b = (E_{water} + E_{gra}) - E_{water/gra}, \quad (2)$$

where the total energies of isolated water, the graphene substrate, and the water–graphene system are E_{water}, E_{gra}, and $E_{water/gra}$, respectively. Within our definition, the preferential adsorption of water on graphene corresponds to a positive value of E_b. The charge rearrangement upon the adsorption of water is defined as

$$\Delta\rho = \rho_{water/gra} - \rho_{water} - \rho_{gra}. \quad (3)$$

Here, $\rho_{water/gra}$, ρ_{water}, and ρ_{gra} are the charge densities of water adsorbed on graphene and of the fragments, *i.e.*, water and graphene in their adsorbed atomic geometries.

3. Results and discussion

3.1. N- and B-doped graphene

Various positions of N and B substitutions for C atoms are shown in Fig. 1. The dopant contents in the graphene sheet are *ca.* 3.1, 6.3, and 9.4% for single, double, and triple site replacement, respectively, and are comparable with the N content in experimentally reported N-doped graphene.[22,39] Formation energies are estimated and summarized in Table 1.

We found that all formation energies are positive, and thus the formation of doped graphene is thermodynamically

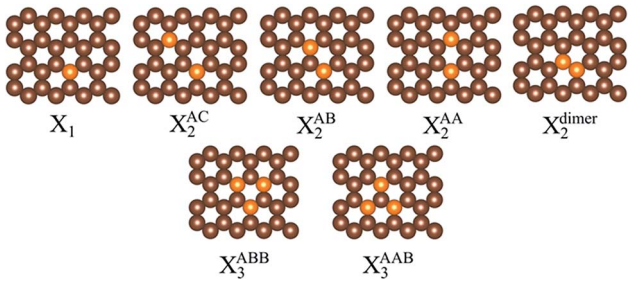

Fig. 1 Atomic configurations of single, double, and triple substitutions with dopant X (X = N, B) in graphene. The positions for the double substitutions are AC, AB, and AA, whereas those for triple substitutions are ABB and AAB. A periodic 4 × 4 supercell of graphene is used. Color scheme: carbon (brown); dopant (orange). Single, double, and triple site doping are denoted by X_1, X_2, and X_3, respectively.

Table 1 Formation energy (E_f), energy difference between the Fermi level and the Dirac point ($\varepsilon_F - \varepsilon_D$), and the work function (ϕ) of doped graphene

N doping				B doping			
Structure	E_f/eV	$\varepsilon_F - \varepsilon_D$/eV	ϕ/eV	Structure	E_f/eV	$\varepsilon_F - \varepsilon_D$/eV	ϕ/eV
N_1	0.885	0.82	3.74	B_1	1.131	−0.87	5.15
N_2^{AC}	1.994	1.24	3.48	B_2^{AC}	2.659	−1.38	5.43
N_2^{AB}	2.187	1.17	3.55	B_2^{AB}	2.788	−1.19	5.36
N_2^{AA}	1.817	1.03	3.72	B_2^{AA}	2.362	−1.14	5.15
N_2^{dimer}	2.815	1.32	3.63	B_2^{dimer}	3.564	−1.19	5.20
N_3^{ABB}	3.414	1.12	3.61	B_3^{ABB}	4.071	−1.30	5.31
N_3^{AAB}	3.566	1.22	3.59	B_3^{AAB}	4.243	−1.32	5.37
Graphene			4.47				

unfavorable with respect to gas-phase N_2, and bulk boron. It should be noted that the calculated positive formation energies are not abnormal, as discussed earlier by Okamoto.[40] Experimentally, N- and B-doped graphene are usually synthesized by the chemical vapor deposition (CVD) method in which the N and B sources are not gas-phase N_2 and bulk boron. For example, double substitution of N in graphene can be achieved by CVD with NH_3 and CH_4 as precursors.[22–26] In addition, the atomic configuration of N- and B-doped graphene can be tuned by using different synthesis methods and a less stable configuration can be obtained.[22–27,40,41] As shown in Table 1, the Fermi level shifts relative to the Dirac point calculated by $\varepsilon_F - \varepsilon_D$ are positive and negative for N- and B-doped graphene, respectively, indicating that N and B doping correspond to n- and p-type doping, respectively. The formation energies of both types of doped graphene increase in the order $X_1 < X_2^{AA} < X_2^{AC} < X_2^{AB} < X_2^{dimer} < X_3^{ABB} < X_3^{AAB}$ (X = N, B), implying that single substitution is preferable in comparison to double and triple substitution. For double site doping by N atoms, the calculated formation energy and $\varepsilon_F - \varepsilon_D$ of N_2^{AA} are the lowest, in good agreement with other theoretical studies.[22,24,40] We found that the formation energies of doped graphene correlate with $\varepsilon_F - \varepsilon_D$; namely the lower perturbation of the π-electrons of graphene results in a more stable configuration, and the observation that higher concentration of dopant results in higher formation energy agrees with the literature.[42–45] Experimentally, the N_2^{AB} configuration was found to be present in more than 80% of N doping sites.[22] In contrast, the calculated formation energy of the N_2^{AB} configuration is greater than that of N_2^{AA} by 0.37 eV, indicating that N_2^{AB} is less stable than N_2^{AA}. Therefore, the positions of the N dopants in graphene strongly depend on the experimental synthesis conditions.[22] For B-doped graphene, the B_1 and B_2^{AA} configurations are found experimentally.[17,25] The B_2^{AA} configuration is synthesized by doping two B atoms into polyaromatic hydrocarbon precursors.[25] B-doped graphene can also be formed by incorporating B atoms within the graphene vacancies.[46] For triple site doping, we consider two doping configurations, namely X_3^{ABB} and X_3^{AAB}, where the dopants alternatively replace the C atoms in graphene. These configurations are similar to the C_3N_4 family, which has proved to have excellent catalytic activity for several important reactions.[47] Here, we don't consider the doping configurations with large distances between the dopant atoms because these configurations cause effects similar to single-site doping.[48]

The work functions of pristine and doped graphene are also listed in Table 1. The work function of pristine graphene is about 4.47 eV which is in good agreement with other theoretical studies (4.38 eV) and experimental values (4.45–4.5 eV).[49] The N- and B-doped systems exhibit lower and higher work functions than pristine graphene and also the BCN monolayer, respectively.[44,49] The different work functions have different effects on the adsorption configuration of water on the substrates, as shown in the below section.

3.2. Water adsorption on graphene substrates

As a reference for the doped systems, the adsorption of water on a pristine graphene substrate was studied. Three stable configurations of water adsorbed on pristine graphene, namely 1-leg, 2-leg, and O-down, were obtained after the geometric optimization (see Fig. 2). The binding energies (E_b), the structural parameters, and the work functions for these three adsorption configurations are summarized in Table 2. We found that 1-leg and 2-leg are more favorable than O-down, implying that the water molecule prefers making H bonds to the pristine graphene surface, and 1-leg is the most favorable structure. Also, the rev-vdW-DF2 functional provided a binding

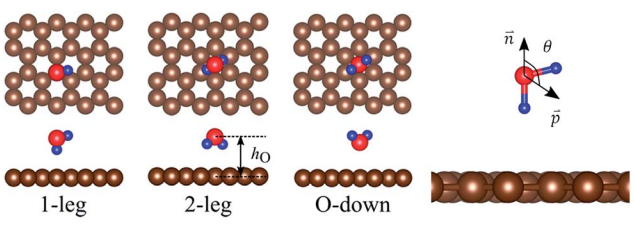

Fig. 2 Adsorption configurations of a water monomer on pristine graphene. A periodic 4 × 4 supercell of graphene was used. Color scheme: carbon (brown), oxygen (red), and hydrogen (blue). The angle (θ) is between the water dipole moment ($\vec{p}$) and the surface normal ($\vec{n}$).

Table 2 Water binding energy (E_b), the vertical bond distance (h_O) from the oxygen atom to the graphene surface, and the angle (θ) between the water dipole moment ($\vec{p}$) and the surface normal ($\vec{n}$) on pristine graphene. The work function (ϕ) and work function change ($\Delta\phi$) relative to the clean surface are also included

Configuration	E_b/meV	h_O/Å	θ/°	ϕ/eV	$\Delta\phi$/eV
1-leg	115	3.38	128	4.86	0.39
	116[a]				
2-leg	110	3.34	178	5.26	0.79
	110[a]				
O-down	99	3.07	3	3.54	−0.93
	101[a]				

[a] The results using a projector augmented wave scheme[50] with an energy cut-off of 80 Ry for the wave function.

energy for water in good agreement with the results obtained by the diffusion Monte Carlo method (100 meV)[8] and the projector augmented wave method.[50] The 1-leg and 2-leg configurations also have a longer vertical bond distance to the surface and a wider dipole moment angle compared to the O-down structure. In addition, the work function variation is positive for 1-leg and 2-leg, while it is negative for the O-down structure.

For the adsorption of H_2O on N- and B-doped graphene, many possible configurations of water were considered. After performing the DFT optimization, the O-down and 1-leg configurations were found on the N- and B-doped substrates, respectively. For each substrate, the most favorable adsorption sites are presented in Fig. 3, and the binding energies are listed in Table 3. Notably, the 2-leg configuration was not found on the N- and B-doped substrates. For single site doping with N, the preferential position of water is on top of the N atom. However, for double and triple site doping with N and all cases of B doping, the water adsorbs stably near the doping atoms. Furthermore, the N-doped substrates retain their planar structure upon water adsorption, while the structure of B_3^{AAB} becomes corrugated, leading to a much higher binding energy. Therefore, we predict that a further increase in the concentration may cause the doped substrates to become unstable towards the adsorption of water.

The binding energies of the water molecule on single site N- and B-doped graphene obtained by the rev-vdW-DF2 functional in the present work are significantly improved compared to those obtained by the GGA-PBE method.[18] Also, they are in good agreement with those obtained by Grimme's D2 method with van der Waals treatment.[20] Single site N and B doping increase the E_b by 39 and 33 meV, respectively, relative to the most favorable configuration (1-leg) on pristine graphene. The order of preference for the adsorption of water on double site N- and B-doped graphene was found to be AB > AC > AA. Doping in the AB positions provides the best substrate for improving the binding energy of H_2O. Noticeably, the AC and AA structures have a higher scattering level of the doping atoms in comparison to the AB structure, and the binding energy of the water molecule on the AC and AA substrates approaches that for single site doping. Therefore, a significant increase in the binding energy can be achieved if the doping atoms are located close together. Also, double site doping with N and B further enhanced the binding energy of H_2O by 33 and 34 meV upon comparing N_2^{AB} and B_2^{AB} to N_1 and B_1, respectively. Notably, triple site N doping (N_3^{AAB}) enhances the binding energy of H_2O by 21 meV compared to the best double site doping (structure N_2^{AB}). In contrast, the B_3^{AAB} substrate increases the binding energy by 98 meV compared to B_2^{AB}. Notably, the B_3^{AAB} structure is deformed by water adsorption. Fig. 4 shows that the binding energy increases almost linearly as a function of doping content at all considered concentrations for N-doped graphene but below 6.3% for B-doped graphene. We estimated that each increase in N and B doping concentration in the linear range could increase the binding energy of H_2O by around 30 meV, indicating that the increase in doping content enhances the water–graphene interaction.

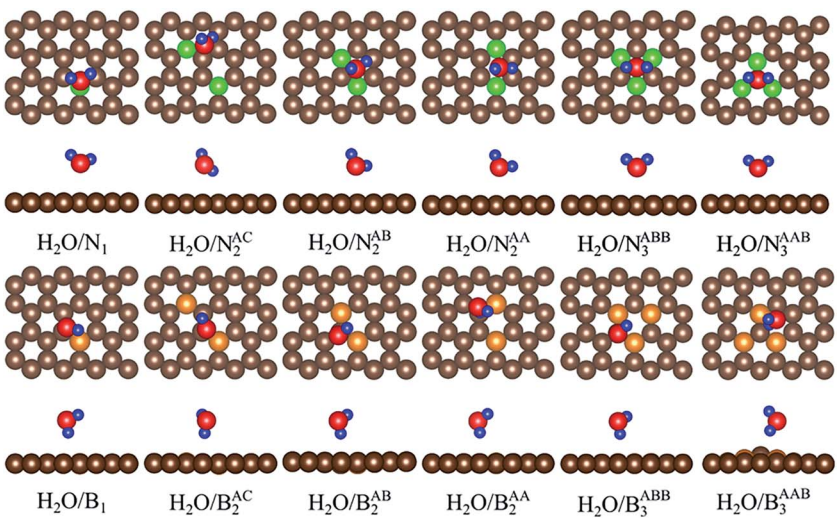

Fig. 3 Adsorption configurations of a water molecule on doped graphene. A periodic 4 × 4 supercell of graphene was used. Color scheme: carbon (brown), nitrogen (green), boron (orange), oxygen (red), and hydrogen (blue).

Table 3 Water binding energy (E_b) and vertical bond distance (h_O) from the oxygen atom to the N- and B-doped graphene. The dipole moment angle (θ), the work function (ϕ), and the work function change ($\Delta\phi$) with respect to the clean surface are also included

N doping						B doping					
Structure	E_b /meV	h_O/Å	θ/°	ϕ/eV	$\Delta\phi$/eV	Structure	E_b /meV	h_O/Å	θ/°	ϕ/eV	$\Delta\phi$/eV
H_2O/N_1	**154** 60[a] 140[b]	**2.97**	**30**	**3.10**	**−0.65**	**H_2O/B_1**	**148** 40[b] 180[b]	**3.30**	**106**	**5.52**	**0.37**
H_2O/N_2^{AC}	163	3.01	42	3.25	−0.23	H_2O/B_2^{AC}	152	3.26	105	5.84	0.41
H_2O/N_2^{AB}	**187**	**2.86**	**12**	**2.90**	**−0.65**	**H_2O/B_2^{AB}**	**182**	**3.10**	**92**	**5.75**	**0.39**
H_2O/N_2^{AA}	160	2.89	30	3.04	−0.68	H_2O/B_2^{AA}	144	3.24	107	5.41	0.26
H_2O/N_3^{ABB}	194	2.80	23	2.79	−0.74	H_2O/B_3^{ABB}	170	3.28	119	5.77	0.05
H_2O/N_3^{AAB}	**208**	**2.85**	**14**	**2.77**	**−0.81**	**H_2O/B_3^{AAB}**	**280**	**2.72[c]**	**89**	**5.51**	**0.13**

[a] GGA-PBE results in ref. 18. [b] PBE + Grimme D2 results in ref. 20. [c] The vertical bond distance between the O of H_2O and the topmost atom of the substrate.

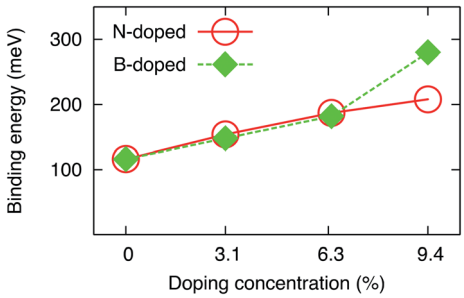

Fig. 4 The binding energy of the water molecule *versus* N and B doping content.

The vertical bond distance from the oxygen atom to the surface decreases from 3.38 > 2.97 > 2.86 ≈ 2.85 Å (3.38 > 3.30 > 3.10 > 2.72 Å) for pristine graphene, N_1, N_2^{AB}, and N_3^{AAB} (pristine graphene, B_1, B_2^{AB}, and B_3^{AAB}), respectively. This trend in the bond distance was found to correlate with the increase in the binding energy. The angle θ of the dipole moment relative to the surface normal is acute and obtuse for the O-down and 1-leg configurations of the water molecule on the N-doped and B-doped substrates, respectively, which have the dipole moment pointing away from and towards the surface, in that order. In addition, the increase in the binding energy was found to closely correlate with the reduction of the dipole moment angle, *i.e.*, 128 > 30 > 12 ≈ 14° (128 > 106 > 92 > 89°) for H_2O on pristine graphene, N_1, N_2^{AB}, and N_3^{AAB} (pristine graphene, B_1, B_2^{AB}, and B_3^{AAB}), respectively. This result implies that the water molecule rotates to minimize the dipole moment angle and stabilize its adsorption on the substrates upon the increase in doping content. The angle change is useful for experiments on static water contact angles.[1–4] Furthermore, the work function decreases and increases relative to the clean surface upon the adsorption of water on N-doped and B-doped graphene, respectively. Also, the work function change $\Delta\phi$ is negative and positive for water on N- and B-doped graphene, respectively, which correlates with the corresponding O-down and 1-leg configurations. The literature showed that the higher the work function, the higher the vacuum level of the substrate should be,[51,52] and therefore, the longer the distance from the surface of the substrate over which the intermolecular forces can take effect on the water molecule. Thus, pristine graphene and B-doped graphene with their high work functions can adsorb water at longer vertical bonding distances (h_O), and hence there is a higher probability of finding the most stable configuration to be the 1-leg structure. Whilst N-doped graphene with its lower work function could only offer the O-down configuration as the most favorable structure, which is located at a shorter vertical bond length. In short, the higher work function of B-doped graphene provides a more extended vacuum space from the substrate surface, allowing the water molecule to orient its structure to form a H bond with the surface, while the lower work function of N-doped graphene only allows the O-down configuration of water to stabilize. It should be noted that the average vertical distance from the water oxygen atom to the surface is shorter for N-doped graphene than B-doped graphene.

In reality, experiments have investigated the adsorption of water monomers and small water clusters *via* STM[13,53] and AFM techniques.[54] Therefore, we also expect that experiments will be set up to confirm our findings on the correlation of the geometrical and physical parameters upon variation of the doping concentration in the considered graphene systems for water adsorption. Our results demonstrated that the increase in doping concentration enhances the water–substrate interaction. Thus, the wettability of graphene is controllable, which is useful for many applications such as electrocatalysis[1,2] and water condensation.[3] For instance, the dissociation of H_2O in the water-splitting reaction becomes easier if the water–graphene interaction increases.

3.3. Electronic structure analysis

Elucidation of the charge rearrangement, the point charges of atoms, and the atomic orbital projected density of states can help us understand the underlying physics determining the interactions of water with the substrates. Fig. 5 shows that the interface regions of O-down H_2O/graphene, H_2O/N_1, H_2O/N_2^{AB}, and H_2O/N_3^{AAB} present charge depletion, while those of 1-leg H_2O/graphene, H_2O/B_1, H_2O/B_2^{AB}, and H_2O/

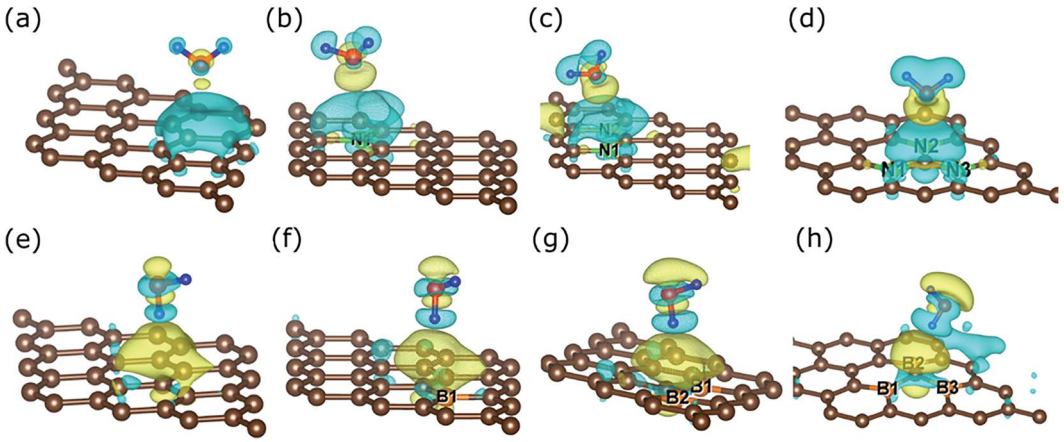

Fig. 5 Charge density difference upon the adsorption of water on the substrate: (a) O-down H_2O/pristine graphene, (b) H_2O/N_1, (c) H_2O/N_2^{AB}, (d) H_2O/N_3^{AAB}, (e) 1-leg H_2O/pristine graphene, (f) H_2O/B_1, (g) H_2O/B_2^{AB}, and (h) H_2O/B_3^{AAB}. Isosurfaces are plotted at 0.0003 e^- $Bohr^{-3}$. Yellow and cyan indicate charge accumulation and depletion, respectively. Color scheme: carbon (brown), nitrogen (green), boron (orange), oxygen (red), and hydrogen (blue).

B_3^{AAB} exhibit charge accumulation. The quantitative charges of each species are given in Table 4. The hydrogen and oxygen atoms of the water always lose and gain charge, respectively. However, the water molecule retains its neutral charge for O-down H_2O/graphene and gains or loses charge for the others. Therefore, the substrate doesn't exchange charge with the water for O-down/graphene, but it exchanges charge with the water for the other structures. The charge exchange is ignorable for the N-doped substrates, but it is significant for the 1-leg H_2O/graphene and the B-doped systems. In addition, the charge exchange for 1-leg H_2O/graphene is higher than that for O-down H_2O/graphene, which explains why the binding energy is higher for the former than the latter. Furthermore, the N atoms accumulate charge while the B atoms donate charge, which is in good agreement with the n-type and p-type nature of N and B doping, respectively. Finally, the obtained binding energies of the water molecule on the different substrates of below 280 meV and the small charge exchange between H_2O and the substrates indicate that the water molecule is physisorbed on the surfaces.

Generally, the interaction between the adsorbate and the substrate is created by the attraction between the unoccupied states of the adsorbate and the occupied states of the substrate, or the occupied states of the adsorbate and the unoccupied states of the substrate.[55] The atomic orbital projected density of states in Fig. 6 shows that an increase in N doping content shifts the C p_z and N p orbitals downward relative to O-down/graphene to increase the occupation at the valence band maximum (VBM). Simultaneously, the lowest unoccupied s orbital (LUMO) of the water also shifts downward towards the Fermi level. Therefore, the energy difference between the LUMO of the water and the VBM decreases in the order: 2.3 > 1.9 > 1.7 > 1.5 eV for the O-down H_2O/graphene, H_2O/N_1, H_2O/N_2^{AB}, and H_2O/N_3^{AAB} structures, respectively. Contrastingly, an increase in B doping concentration shifts the C p_z and B p orbitals upward towards the Fermi level to increase the unoccupied states at the conduction band minimum (CBM) of the substrate. Simultaneously, the highest occupied peak of the water p orbital (HOMO) moves upward to reduce the energy difference between the HOMO and the CBM to 2.6 > 1.9 > 1.5 ≈ 1.5 eV for the 1-leg H_2O/graphene, H_2O/B_1, H_2O/B_2^{AB}, and H_2O/B_3^{AAB} configurations, respectively. The reduction of the energy differences between the LUMO of water and the VBM of the substrate, and the HOMO of water and the CBM of the substrate was found to correlate with the enhancement of the water binding energy. Furthermore, the position of the p orbital peak of the 1-leg configuration is also closer to the Fermi level than that of the O-down configuration. Therefore, the interaction of the water molecule with the substrate is stronger for the 1-leg structure than the O-down structure.

Table 4 Bader charges (in *e*) of the atoms

H_2O/substrate	O-down H_2O/graphene	H_2O/N_1	H_2O/N_2^{AB}	H_2O/N_3^{AAB}	1-leg H_2O/graphene	H_2O/B_1	H_2O/B_2^{AB}	H_2O/B_3^{AAB}
2H	−1.259	−1.170	−1.618	−1.243	−1.169	−1.245	−1.231	−1.275
O	1.259	1.175	1.624	1.234	1.183	1.265	1.253	1.306
H_2O	**0.000**	**0.005**	**0.006**	**−0.009**	**0.014**	**0.020**	**0.022**	**0.031**
C atoms	0.000	−1.115	−5.248	−8.365	−0.014	2.980	5.978	8.969
N (B) atoms		1.110	5.242	8.375		−3.000	−6.000	−9.000
Substrate	**0.000**	**−0.005**	**- 0.006**	**0.009**	**−0.014**	**−0.020**	**−0.022**	**−0.031**

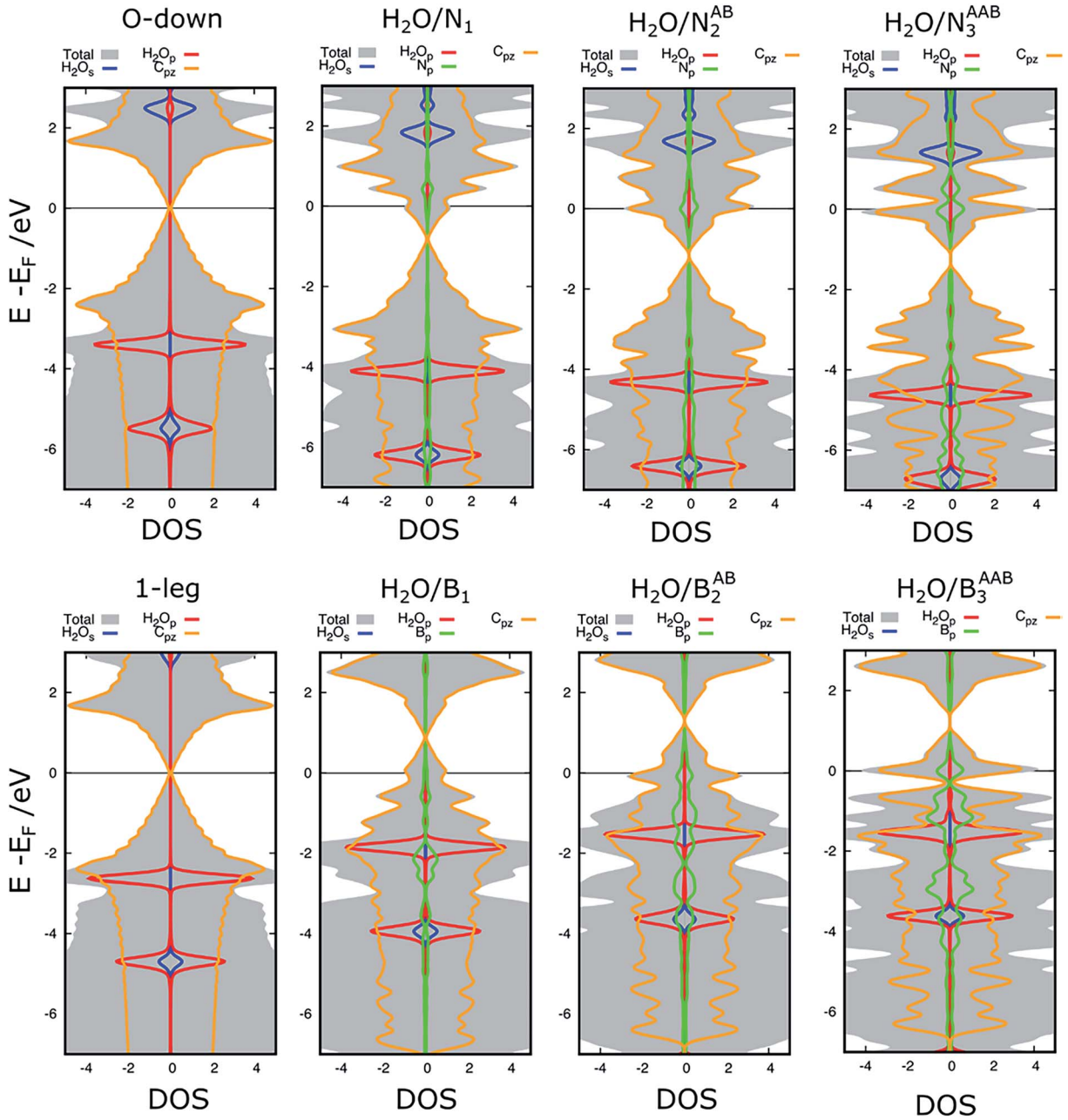

Fig. 6 Atomic orbital projected density of states of water in the O-down and 1-leg configurations on pristine graphene and on N- and B-doped graphene.

4. Conclusions

Density functional theory calculations with the rev-vdW-DF2 functional have been used to explore the effects of N and B doping and also the doping concentration in graphene on water adsorption. The most favorable adsorption configurations of water are O-down and 1-leg for the N and B dopants, respectively. The increase in doping content enhances the binding energy of water. The increase in doping concentration enriches the occupied states at the VBM for N doping and the unoccupied states at the CBM for B doping, which originates from the corresponding contributions of the C p_z and N p orbitals and the C p_z and B p orbitals, respectively. Simultaneously, with increasing doping content, the unoccupied s orbital (LUMO) of water shifts closer to the VBM of N-doped graphene, while the occupied p orbital (HOMO) of water moves closer to the CBM of B-doped graphene. This shift reduces the energy gap, favors the water–graphene interaction, and hence improves the water binding energy. Furthermore, the water molecule was found to rotate its structure to minimize the dipole moment angle relative to the surface normal upon increasing the doping content.

Conflicts of interest

There are no conflicts of interest to declare.

Acknowledgements

This research was funded by Vietnam National University Ho Chi Minh City under grant number C2020-20-39.

References

1 D. Parobek and H. Liu, Wettability of graphene, *2D Mater.*, 2015, **2**, 032001.
2 C. Melios, C. E. Giusca, V. Panchal and O. Kazakova, Water on graphene: review of recent progress, *2D Mater.*, 2018, **5**, 022001.
3 G. Hong, Y. Han, T. M. Schutzius, Y. Wang, Y. Pan, M. Hu, J. Jie, C. S. Sharma, U. Müller and D. Poulikakos, On the Mechanism of Hydrophilicity of Graphene, *Nano Lett.*, 2016, **16**, 4447.
4 A. Ashraf, Y. Wu, M. C. Wang, K. Yong, T. Sun, Y. Jing, R. T. Haasch, N. R. Aluru and S. Nam, Doping-Induced Tunable Wettability and Adhesion of Graphene, *Nano Lett.*, 2016, **16**, 4708.
5 O. Leenaerts, B. Partoens and F. M. Peeters, Water on graphene: hydrophobicity and dipole moment using density functional theory, *Phys. Rev. B*, 2009, **79**, 235440.
6 I. Hamada, Adsorption of water on graphene: a van der Waals density functional study, *Phys. Rev. B: Condens. Matter Mater. Phys.*, 2012, **86**, 195436.
7 A. O. Ajala, V. Voora, N. Mardirossian, F. Furche and F. Paesani, Assessment of Density Functional Theory in Predicting Interaction Energies between Water and Polycyclic Aromatic Hydrocarbons: from Water on Benzene to Water on Graphene, *J. Chem. Theory Comput.*, 2019, **15**, 2359.
8 J. G. Brandenburg, A. Zen, M. Fitzner, B. Ramberger, G. Kresse, T. Tsatsoulis, A. Grüneis, A. Michaelides and D. Alfè, Physisorption of Water on Graphene: Subchemical Accuracy from Many-Body Electronic Structure Methods, *J. Phys. Chem. Lett.*, 2019, **10**, 358.
9 T. O. Wehling, A. I. Lichtenstein and M. I. Katsnelson, First-principles studies of water adsorption on graphene: the role of the substrate, *Appl. Phys. Lett.*, 2008, **93**, 202110.
10 G. Revilla-López and N. López, A unified study for water adsorption on metals: meaningful models from structural motifs, *Phys. Chem. Chem. Phys.*, 2014, **16**, 22426.
11 J. E. Andrews, S. Sinha, P. W. Chung and S. Das, Wetting dynamics of a water nanodrop on graphene, *Phys. Chem. Chem. Phys.*, 2016, **18**, 23482.
12 A. Akaishi, T. Yonemaru and J. Nakamura, Formation of Water Layers on Graphene Surfaces, *ACS Omega*, 2017, **2**, 2184.
13 Y.-R. Wang, J.-Y. Xu, C.-K. Ma, M.-X. Shi, Y.-B. Tu, K. S. S. Meng and J.-Z. Wang, Ice II-like Monolayer Ice Grown on Graphite Surface, *J. Phys. Chem. C*, 2019, **123**, 20297–20303.
14 J. Fujiki and K. Yogo, Water adsorption on nitrogen-doped carbons for adsorption heat pump/desiccant cooling: Experimental and density functional theory calculation studies, *Appl. Surf. Sci.*, 2019, **492**, 776.
15 K. V. Kumar, K. Preuss, Z. X. Guo and M. M. Titirici, Understanding the Hydrophilicity and Water Adsorption Behavior of Nanoporous Nitrogen-Doped Carbons, *J. Phys. Chem. C*, 2016, **120**, 18167.
16 N.-J. Kuo, Y.-S. Chen, C.-W. Wu, C.-Y. Huang, Y.-H. Chan and I. P. Chen, One-Pot Synthesis of Hydrophilic and Hydrophobic N-Doped Graphene Quantum Dots *via* Exfoliating and Disintegrating Graphite Flakes, *Sci. Rep.*, 2016, **6**, 30426.
17 S. Agnoli and M. Favaro, Doping graphene with boron: a review of synthesis methods, physicochemical characterization, and emerging applications, *J. Mater. Chem. A*, 2016, **4**, 5002.
18 J. Dai, J. Yuan and P. Giannozzi, Gas adsorption on graphene doped with B, N, Al, and S: a theoretical study, *Appl. Phys. Lett.*, 2009, **95**, 232105.
19 Y. Yang, F. Liu and Y. Kawazoe, Adsorptionof water on fluorinated graphene, *J. Phys. Chem. Solids*, 2019, **124**, 54.
20 A. Xu, L. Shi, L. Zeng and T. S. Zhao, First-principle investigations of nitrogen-, boron-, phosphorus-doped graphite electrodes for vanadium redox flow batteries, *Electrochim. Acta*, 2019, **300**, 389.
21 V. A. Cardozo–Mata, J. A. Pescador–Rojas, A. Hernández–Hernández, L. A. Hernández–Hernández, A. Miralrio, F. J. M. Farías, E. Vallejo–Castañeda and E. Rangel, Chemical interaction between nitrogen-doped graphene defects and a copper (111) surface: Effects on water molecule adsorption, *Appl. Surf. Sci.*, 2020, **502**, 144149.
22 R. Lv, Q. Li, A. R. Botello-Méndez, T. Hayashi, B. Wang, A. Berkdemir, Q. Hao, A. L. Elías, R. Cruz-Silva, H. R. Gutiérrez, Y. A. Kim, H. Muramatsu, J. Zhu, M. Endo, H. Terrones, J.-C. Charlier, M. Pan and M. Terrones, Nitrogen-doped graphene: beyond single substitution and enhanced molecular sensing, *Sci. Rep.*, 2012, **2**, 586.
23 D. Deng, X. Pan, L. Yu, Y. Cui, Y. Jiang, J. Qi, W.-X. Li, Q. Fu, X. Ma, Q. Xue, G. Sun and X. Bao, Toward N-Doped Graphene *via* Solvothermal Synthesis, *Chem. Mater.*, 2011, **23**, 1188.
24 Y.-X. Yu, Can all nitrogen-doped defects improve the performance of graphene anode materials for lithium-ion batteries?, *Phys. Chem. Chem. Phys.*, 2013, **15**, 16819.
25 C. Dou, S. Saito, K. Matsuo, I. Hisaki and S. Yamaguchi, A Boron-Containing PAH as a Substructure of Boron-Doped Graphene, *Angew. Chem., Int. Ed.*, 2012, **51**, 12206–12210.
26 C. Ma, Q. Liao, H. Sun, S. Lei, Y. Zheng, R. Yin, A. Zhao, Q. Li and B. Wang, Tuning the Doping Types in Graphene Sheets by N Monoelement, *Nano Lett.*, 2018, **18**, 386.
27 P. Błoński, J. Tuček, Z. Sofer, V. Mazánek, M. Petr, M. Pumera, M. Otyepka and R. Zbořil, Doping with Graphitic Nitrogen Triggers Ferromagnetism in Graphene, *J. Am. Chem. Soc.*, 2017, **139**, 3171.
28 H. Wang, T. Maiyalagan and X. Wang, Review on Recent Progress in Nitrogen-Doped Graphene: Synthesis, Characterization, and Its Potential Applications, *ACS Catal.*, 2012, **2**, 781.
29 P. Giannozzi, O. Andreussi, T. Brumme, O. Bunau, M. B. Nardelli, M. Calandra, R. Car, C. Cavazzoni, D. Ceresoli, M. Cococcioni, N. Colonna, I. Carnimeo,

A. D. Corso, S. de Gironcoli, P. Delugas, R. A. DiStasio, A. Ferretti, A. Floris, G. Fratesi, G. Fugallo, R. Gebauer, U. Gerstmann, F. Giustino, T. Gorni, J. Jia, M. Kawamura, H.-Y. Ko, A. Kokalj, E. Küçükbenli, M. Lazzeri, M. Marsili, N. Marzari, F. Mauri, N. L. Nguyen, H.-V. Nguyen, A. Otero-de-la-Roza, L. Paulatto, S. Poncé, D. Rocca, R. Sabatini, B. Santra, M. Schlipf, A. P. Seitsonen, A. Smogunov, I. Timrov, T. Thonhauser, P. Umari, N. Vast, X. Wu and S. Baroni, Advanced capabilities for materials modelling with Quantum ESPRESSO, *J. Phys.: Condens. Matter*, 2017, **29**, 465901.

30 D. Vanderbilt, Soft self-consistent pseudopotentials in a generalized eigenvalue formalism, *Phys. Rev. B: Condens. Matter Mater. Phys.*, 1990, **41**, 7892.

31 K. F. Garrity, J. W. Bennett, K. M. Rabe and D. Vanderbilt, Pseudopotentials for high-throughput DFT calculations, *Comput. Mater. Sci.*, 2014, **81**, 446.

32 I. Hamada, van der Waals density functional made accurate, *Phys. Rev. B: Condens. Matter Mater. Phys.*, 2014, **89**, 121103.

33 J. G. Brandenburg, A. Zen, D. Alfè and A. Michaelides, Interaction between water and carbon nanostructures: how good are current density functional approximations?, *J. Chem. Phys.*, 2019, **151**, 164702.

34 T. N. Pham, M. Sugiyama, F. Muttaqien, S. E. M. Putra, K. Inagaki, D. N. Son, Y. Hamamoto, I. Hamada and Y. Morikawa, Hydrogen Bond-Induced Nitric Oxide Dissociation on Cu(110), *J. Phys. Chem. C*, 2018, **122**, 11814.

35 T. N. Pham, Y. Hamamoto, K. Inagaki, D. N. Son, I. Hamada and Y. Morikawa, Insight into Trimeric Formation of Nitric Oxide on Cu(111): A Density Functional Theory Study, *J. Phys. Chem. C*, 2020, **124**, 2968.

36 N. T. X. Huynh, V. Chihaia and D. N. Son, Hydrogen storage in MIL-88 series, *J. Mater. Sci.*, 2019, **54**, 3994–4010.

37 D. N. Son, T. T. T. Huong and V. Chihaia, Simultaneous adsorption of SO_2 and CO_2 in an Ni(bdc)(ted)$_{0.5}$ metal–organic framework, *RSC Adv.*, 2018, **8**, 38648.

38 L. Bengtsson, Dipole correction for surface supercell calculations, *Phys. Rev. B: Condens. Matter Mater. Phys.*, 1999, **59**, 12301.

39 S. Yang, L. Zhi, K. Tang, X. Feng, J. Maier and K. Müllen, Efficient Synthesis of Heteroatom (N or S)-Doped Graphene Based on Ultrathin Graphene Oxide–Porous Silica Sheets for Oxygen Reduction Reactions, *Adv. Funct. Mater.*, 2012, **22**, 3634.

40 Y. Okamoto, First-principles molecular dynamics simulation of O_2 reduction on nitrogen-doped carbon, *Appl. Surf. Sci.*, 2009, **256**, 335.

41 M. Telychko, P. Mutombo, P. Merino, P. Hapala, M. Ondráček, F. C. Bocquet, J. Sforzini, O. Stetsovych, M. Vondráček, P. Jelínek and M. Švec, Electronic and Chemical Properties of Donor, Acceptor Centers in Graphene, *ACS Nano*, 2015, **9**, 9180.

42 S. Thomas and M. A. Zaeem, A new planar BCN lateral heterostructure with outstanding strength and defect-mediated superior semiconducting to metallic properties, *Phys. Chem. Chem. Phys.*, 2020, **22**, 22066.

43 S. Beniwal, J. Hooper, D. P. Miller, P. S. Costa, G. Chen, S.-Y. Liu, P. A. Dowben, E. C. H. Sykes, E. Zurek and A. Enders, Graphene-like Boron–Carbon–Nitrogen Monolayers, *ACS Nano*, 2017, **11**, 2486.

44 S. Thomas, M. S. Manju, K. M. Ajith, S. U. Lee and M. Asle Zaeem, Strain-induced work function in h-BN and BCN monolayers, *Phys. E*, 2020, **123**, 114180.

45 S. Thomas and S. U. Lee, Atomistic insights into the anisotropic mechanical properties and role of ripples on the thermal expansion of h-BCN monolayers, *RSC Adv.*, 2019, **9**, 1238.

46 R. Lv, G. Chen, Q. Li, A. McCreary, A. Botello-Méndez, S. V. Morozov, L. Liang, X. Declerck, N. Perea-López, D. A. Cullen, S. Feng, A. L. Elías, R. Cruz-Silva, K. Fujisawa, M. Endo, F. Kang, J.-C. Charlier, V. Meunier, M. Pan, A. R. Harutyunyan, K. S. Novoselov and M. Terrones, Ultrasensitive gas detection of large-area boron-doped graphene, *Proc. Natl. Acad. Sci. U. S. A.*, 2015, **112**, 14527.

47 W. J Ong, L. L. Tan, Y. H. Ng, S. T. Yong and S. P. Chai, Graphitic Carbon Nitride (g-C_3N_4)-Based Photocatalysts for Artificial Photosynthesis and Environmental Remediation: Are We a Step Closer To Achieving Sustainability?, *Chem. Rev.*, 2016, **116**, 7159.

48 T. M. Dieb, Z. Hou and K. Tsuda, Structure prediction of boron-doped graphene by machine learning, *J. Chem. Phys.*, 2018, **148**, 241716.

49 M. Legesse, F. El Mellouhi, E. T. Bentria, M. E. Madjet, T. S. Fisher, S. Kais and F. H. Alharbi, Reduced work function of graphene by metal adatoms, *Appl. Surf. Sci.*, 2017, **394**, 98.

50 P. E. Blöchl, Projector augmented-wave method, *Phys. Rev. B: Condens. Matter Mater. Phys.*, 1994, **50**, 17953.

51 D. N. Son, B. T. Cong and H. Kasai, Hydronium Adsorption on OOH Precovered Pt(111) Surface: Effects of Electrode Potential, *J. Nanosci. Nanotechnol.*, 2011, **11**, 2983–2989.

52 D. N. Son, P. V. Cao, T. T. T. Hanh, V. Chihaia and M. P. Pham-Ho, Influences of Electrode Potential on Mechanism of Oxygen Reduction Reaction on Pd-Skin/Pd_3Fe(111) Electrocatalyst: Insights from DFT-Based Calculations, *Electrocatalysis*, 2018, **9**, 10–21.

53 C. L. Muhich, J. Y. Westcott, T. C. Morris, A. W. Weimer and C. B. Musgrave, The effect of N and B doping on graphene and the adsorption and migration behavior of Pt atoms, *J. Phys. Chem. C*, 2013, **117**, 10523.

54 T. Kumagai, M. Kaizu, H. Okuyama, S. Hatta, T. Aruga, I. Hamada and Y. Morikawa, Direct Observation of Hydrogen-Bond Exchange within a Single Water Dimer, *Phys. Rev. Lett.*, 2008, **100**, 166101.

55 O. K. Le, V. Chihaia, M. P. Pham-Ho and D. N. Son, Electronic and optical properties of monolayer MoS_2 under the influence of polyethyleneimine adsorption and pressure, *RSC Adv.*, 2020, **10**, 4201–4210.